

Full Length Article

Influence of geometry on proximal femoral shaft strains: Implications for atypical femoral fracture

Ifaz T. Haider^{a,b,*}, Prism Schneider^{b,c}, Andrew Michalski^{b,d}, W. Brent Edwards^{a,b,d}^a Human Performance Laboratory, Faculty of Kinesiology, University of Calgary, 2500 University Dr. NW, Calgary, Alberta T2N 1N4, Canada^b McCaig Institute for Bone and Joint Health, University of Calgary, HRC 3A08, 3280 Hospital Drive NW, Calgary, Alberta T2N 4Z6, Canada^c Department of Surgery, Department of Community Health Sciences, Cumming School of Medicine, Foothills Campus, University of Calgary, 3330 Hospital Drive NW, Calgary, Alberta T2N 4N1, Canada^d Biomedical Engineering Graduate Program, University of Calgary, 2500 University Dr. NW, Calgary, Alberta T2N 1N4, Canada

ARTICLE INFO

Article history:

Received 30 October 2017

Revised 25 January 2018

Accepted 17 February 2018

Available online 23 February 2018

Keywords:

Atypical femoral fracture

Finite element modelling

Bone mechanics

ABSTRACT

Introduction: Atypical femoral fractures (AFF) are characterized as low-energy fractures of the femoral shaft or subtrochanteric region. Femoral geometry is known to play a role in AFF risk; it is hypothesized that high-risk geometries are associated with elevated femoral shaft strain. However, it is not well known which geometric parameters have the greatest effect on strain, or whether interaction between parameters is significant. The purpose of this study was to thoroughly quantify the relationship between femoral geometry and diaphyseal strain, using patient specific finite element (FE) modelling in concert with parametric mesh morphing.

Methods: Ten FE models were generated from computed tomography (CT) images of cadaveric femora. Heterogeneous material properties were assigned based on average CT intensities at element locations and models were subject to loads and boundary conditions representing the stance phase of gait. Mesh morphing was used to manipulate 8 geometric parameters: neck shaft angle (NSA), neck version angle (NV), neck length (NL), femoral length (FL), lateral bowing angle (L.Bow), anterior bowing angle (A.Bow), shaft diameter (S.Dia), and cortical bone thickness (C.Th). A 2-Level full factorial analysis was used to explore the effect of different combinations of physiologically realistic minimum and maximum values for each parameter. Statistical analysis (Generalized Estimating Equations) was used to assess main effects and first order interactions of each parameter.

Results: Six independent parameters and seven interaction terms had statistically significant ($p < 0.05$) effects on peak strain and strained volume. For both measures, the greatest changes were caused by S.Dia, L.Bow, and A. Bow, and/or first order interactions involving two of these variables.

Conclusions: As hypothesized, a large number of geometric measures (six) and first order interactions (seven) are associated with changes in femoral shaft strain. These measures can be evaluated radiographically, which may have important implications for future studies investigating AFF risk in clinical populations.

© 2017 Elsevier Inc. All rights reserved.

1. Introduction

At least one in three women and one in five men will suffer from an osteoporotic (OP) fracture during their lifetime [1]. The mainstay of osteoporosis (OP) treatment has been antiresorptive therapy, such as bisphosphonates (BP) and these medications have been proven to reduce hip and spine fractures [2,3]. However, recent reports have also noted that prolonged use of BPs may be associated with rare but serious atypical femoral fractures (AFF), characterized as fractures of the

femoral shaft or subtrochanteric region, which typically occur in the absence of notable trauma [4].

The etiology of AFF is not fully understood. Unlike more common fragility fractures of femoral neck or trochanteric region, AFF occurs in what is typically the strongest part of the proximal femur. It has been suggested that mechanical fatigue effects, rather than acute overloading, may play an important role in AFF fractures. The prevailing hypothesis suggests suppressed bone remodeling, associated with prolonged BP treatment, may alter bone material properties and/or inhibit the bone's ability to repair microdamage. In either case, these effects could allow for damage to more easily accumulate until a fatigue fracture occurs [5–8]. As the onset of prodromal pain and radiographic changes can be insidious [4], it would be beneficial to identify patients at high risk for AFF, who would benefit most from additional screening,

* Corresponding author at: Human Performance Laboratory, Faculty of Kinesiology, University of Calgary, 2500 University Dr. NW, Calgary, Alberta T2N 1N4, Canada.

E-mail address: ifaz.haider@ucalgary.ca (I.T. Haider).

treatment interruption, or prophylactic fixation, without influencing treatment in the majority who benefit from BP medication [1,9].

To this end, recent studies have sought to identify clinical risk factors for AFF [10–16], and a number of these studies have found associations between femoral geometry and the development of AFF. It has been observed that patients with AFF have more varus neck-shaft angles [13], and greater lateral bowing of the femoral diaphysis [11], compared to unfractured controls. However, it is unclear whether additional geometric parameters are important, or whether a combination of geometric measures interacts to increase fracture risk. The rarity of AFF makes it challenging to answer these questions using epidemiological means alone. Therefore, a mechanistic approach may provide additional insight.

It is commonly hypothesized that geometry influences AFF risk by increasing mechanical strains at the femoral shaft [6,10,11,14–16]. In order to investigate this hypothesis further, it is necessary to more thoroughly explore the relationship between femoral geometry and femoral strains. This can be accomplished effectively using patient-specific finite element (FE) modelling, wherein geometry and material properties obtained from quantitative computed tomography (QCT) is used to generate 3D models that accurately predict the structural response of the bones [17–19]. However, it would be extremely challenging to identify, image and model a group of patients whose femoral geometries cover the full range of variation possible in the population. Instead, once a patient-specific model is generated, mesh-morphing techniques can be used to parametrically manipulate model geometry. These methods identify a set of important landmarks on the surface of the FE models, and prescribe a deformation (displacement) to each landmark. The morphed positions of all other points on the model are then computed by interpolation. In the past, these methods have often been used to generate specimen-specific models from generic mesh templates [20], but the technique can be extended to allow user-specified manipulation of individual geometric parameters [21].

The purpose of this study was to thoroughly quantify the relationship between femoral geometry and proximal femoral strain. This was done using patient-specific FE modelling to simulate the structural response of the femur under walking load conditions. To this end, a novel mesh morphing technique was developed in order to manipulate femoral geometry, and to examine how different geometric parameters interact to influence femoral shaft strain. These results may inform future clinical investigations, and ultimately result in improved techniques for early identification of AFF risk.

2. Methods

2.1. Patient-specific FE modelling

An initial set of 10 patient-specific FE models of the femur were generated from QCT scans of human cadavers (Mean Age = 81.8, 6 males, 4 females). Scans were performed using a GE Revolution GSI (GE Healthcare), with acquisition settings of 120 kVp, 103 mA, an in-plane resolution of 0.67×0.67 mm, and slice thickness of 0.625 mm. A K_2HPO_4 calibration phantom (Mindways Software, Inc., Model 3, Austin, TX, USA) was placed in the field of view; this allowed bone apparent density to be estimated from image intensity values. The Materialise Mimics Innovation Suite (Materialise, Leuven, Belgium) of commercial software was used to manually segment bone voxels from QCT images, and generate a tetrahedral volume mesh. Models were generated with an average surface element edge length of 3.5 mm, resulting in 270,000 to 380,000 second-order tetrahedral elements. One of the models was refined in order to test convergence of the mesh. Increasing the number of elements by 50% changed peak surface strain prediction by <1%.

The femur bone was modeled as an isotropic material with a Poisson's ratio of 0.3 [22–24] and spatially varying Young's modulus. Mimics software was used to compute the average CT Hounsfield unit

(HU) within each element. The element averaged HU was then related to a K_2HPO_4 equivalent density by linear regression using the measured HU values in the phantom compared to known density values provided by the manufacturer's certificate. The elastic modulus, E , of each element was assigned using a density-modulus relationship specific to femoral bone:

$$E = 6850\rho_{app}^{1.49} \quad (1)$$

where E is the Young's modulus in MPa and ρ_{app} is the apparent density in g/cm^3 . This relationship has been validated previously, and produced a strong linear correlation ($R^2 = 0.911$) between model predicted and experimentally measured strain [25]. K_2HPO_4 equivalent density, computed from the phantom, was related to ash density using previously reported correlations [26] then divided by a factor of 0.6 in order to compute bone apparent density [25].

The FE models were subject to physiological loads and boundary conditions, representing the first peak load during the stance phase of gait (Fig. 1). Muscle and contact forces had been computed previously by Edwards et al. [27], using a forward dynamics approach. These forces were applied as point loads to the femoral head and at each muscle insertion point. For each model in this study, muscle insertion nodes were also identified by comparison to the previous model from Edwards et al. [27]. The two models were non-rigidly aligned using an iterative closest point algorithm, implemented in CloudCompare software (open-source, <http://www.danielgm.net/cc/>). After alignment, each muscle attachment node from the original FE model was mapped to the nearest surface node of the new FE model. The nonrigid transformation was discarded after muscle insertion nodes were identified.

The femur was fully constrained at a single point at the center of the distal condyles, while the point of loading on the head was constrained to motion along the proximal-distal axis only. A single point on the lateral condyle was also constrained to restrict motion along the anterior-posterior axis. Together, these constraints model a pair of pin joints, which allow free rotation of the proximal and distal ends while constraining rigid body translation. The combination of boundary constraints, hip contact force, and muscle forces used in this work was previously examined by Edwards et al. [27], who reported that this set of BCs generated physiologically realistic deformations of the femoral shaft which were consistent with previous FE simulations [28,29] and in-vivo measurements of strain [30].

To the best of the author's knowledge, there are no validated organ-level FE models, which predict the fatigue life of whole human bones. In this study, relevant measures were selected based on the engineering principles which have been explored through material level tests [31–38]. As it is well established that fatigue life is highly dependent on strain magnitude [38], peak femoral strain was used as one indicator of fracture risk. Bones at the organ level are, however, in a complex state of loading, with different combinations of tension, compression and shear depending on anatomic site. An equivalent strain criterion is typically used to facilitate comparison between failure at different loading regimes [39], but relatively few studies have explored the use of different equivalent strain measurements for the prediction of fatigue life in bone. In this study, we adopted the equivalent von Mises Strain criterion, which has been used with some success in the past [36].

Peak strain alone, however, may be an insufficient criterion for assessing fatigue fracture risk [5]. Fatigue fracture is the eventual result of crack nucleation and propagation. Localized stress concentrators, such as pre-existing damage or differences in the size and shape of vascular canals, may play an important role in specimen fatigue life. However, these cannot be assessed at clinical CT resolutions. For this reason, strained volume was also measured in this work, as femoral geometry with a larger strained volume increases the probability of significant loading at sensitive sites [40].

Strains were evaluated at volume elements located on the surface of the femur. The region of interest was further limited to the proximal half

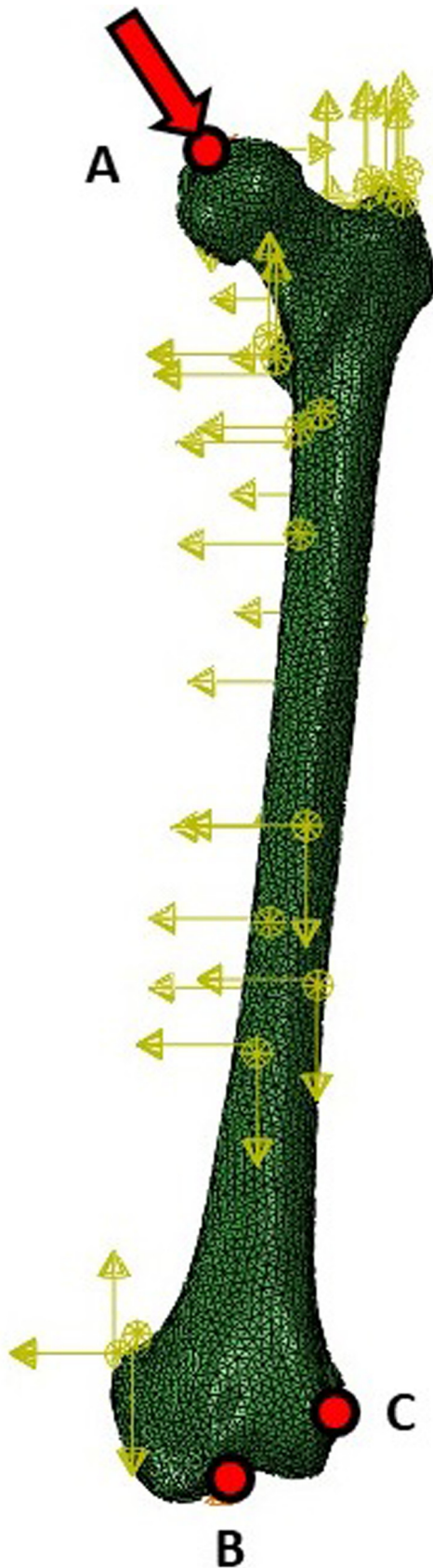


Fig. 1. Loads and BCs, adopted from [27], applied to a femoral mesh. Hip contact force was applied at point A, which was constrained to only allow motion in the proximal-distal direction. One node at the center of the knee (B) was fully fixed in all directions. Finally, a node on the lateral condyle (C) was constrained to restrict motion in the anterior-posterior direction.

of the femoral diaphysis, between the midshaft and the distal end of the lesser trochanter (Fig. 2). Linear models can exhibit highly localized strains, which may be artefactual, and these potential errors were resolved by averaging strains over a 3 mm radius [23]. After averaging, peak von Mises equivalent strain was quantified.

It has been noted in the literature that AFF typically occurs at one of two different vertical locations, either the midshaft or subtrochanteric region of the femur [14,41]. In this study, we compared the vertical location of peak von Mises strain in order to determine whether femoral geometry could influence fracture location. To facilitate comparison between different femora, we normalized our reported vertical coordinates with respect to the length of the region of interest, i.e., 0% indicating peak strain at the base of the lesser trochanter and 100% indicating peak strain at the midshaft (Fig. 2).

Finally, we also evaluated changes to highly strained volume. This was done by generating a histogram of strains from all surface elements in the proximal shaft. Strained volume was reported as the volume of all elements in the upper 4th quartile divided by the total volume of all elements in the histogram. For this calculation, extraneous localized effects were handled by removing the top 1% from the calculation of quartile ranges. These elements, however, still contribute to the total strained volume reported.

2.2. Mesh morphing

Geometry of the 10 patient-specific models, described above, was manipulated in order to assess the influence of geometric changes on femoral shaft strains. This was done using a custom mesh morphing algorithm that was implemented in MATLAB (v.R2016a, Mathworks, Massachusetts, United States). As input, the user first identified all surface nodes located in one of four regions: the femoral head, femoral neck, femoral diaphysis, and distal condyles. The algorithm automatically down-sampled each list to a more manageable set of surface landmarks, with approximately 150 points at the head, 150 at the neck, 500 at the periosteal surface of the femoral shaft, and 100 at the distal condyles (Fig. 2). For each of the 500 points on the femoral shaft, the MATLAB algorithm generated an additional landmark near the endosteal surface. This point was on the same axial plane as the user-selected periosteal landmark, and the distance between the two points was equal to the average cortical thickness of the bone. The number of points was determined based on trial and error; the final numbers reported here allowed the algorithm to morph the models without generating any obvious artefact or abnormalities.

The custom MATLAB algorithm computed new positions for these surface landmarks, in order to achieve a user-specified target geometry. This geometry was defined by eight parameters: neck shaft angle (NSA), neck version angle (NV), neck length (NL), femoral length (FL), lateral bowing angle (L.Bow), anterior bowing angle (A.Bow), shaft diameter (S.Dia), and cortical bone thickness (C.Th). As shown in Table 1, NSA was the angle between the femoral neck axis and the axis of the proximal shaft in the coronal plane [42]. NV was the angle between the femoral neck axis and the medial-lateral axis in the transverse plane [43]. In both cases, the neck axis was identified by a line passing through the center of the femoral head and the centroid of the thinnest cross section of the neck. NL was measured as the shortest distance between the inferior base of the femoral head to the medial end of the intertrochanteric line. FL was measured as the vertical distance between the most proximal point of the femoral head and the most distal point of the condyles [42]. L.Bow was the angle between the local shaft axes at 20% and 80% of the total length in the coronal plane. Bowing in the lateral direction was defined as positive. Similarly, A.Bow was the angle between the local shaft axes, at the same locations, but viewed in the sagittal plane. In this case, anterior bowing was defined as positive. S.Dia was the average diameter of the periosteal surface, measured at the midshaft, while C.Th was the difference between the diameter of the periosteal and endosteal surfaces at the same location. Noting that the bone is not a perfect circle,

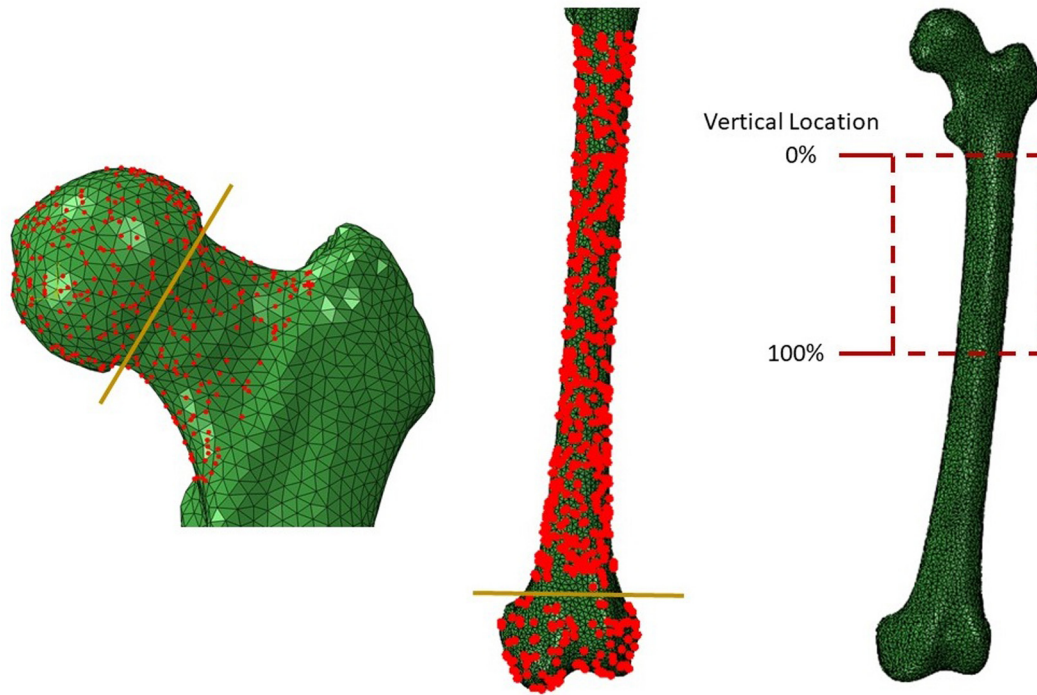


Fig. 2. Visualization of landmark nodes and analysis region of interest. LEFT: 150 nodes were identified on the femoral head, and another 150 were selected from the femoral shaft. CENTER: 500 nodes were selected on the surface of the shaft, while another 100 nodes were selected from the distal condyles. A yellow line was used to depict the separation of regions. RIGHT: Von Mises Strains were analyzed in the proximal half of the femoral shaft, highlighted in the figure with a dotted red line. The vertical location of peak strain was also analyzed. To facilitate comparison, vertical coordinates were normalized with respect to the length of this region of interest; i.e., 0% at the base of the lesser trochanter and 100% at the midshaft. For additional clarity, readers are referred to the online colour publication.

diameter was measured in both the anterior-posterior and medial-lateral directions, then averaged [44].

Once the surface landmarks are warped, the locations of all other nodes (surface and internal) of the model were computed as follows. Let $i = 1 \dots n$, denote the landmark points, and $I = 1 \dots N$ denote all other nodes in the mesh. Each i th landmark position was associated with a known original position $\mathbf{p}_i = (x_i, y_i, z_i)$, and a warped position $\mathbf{p}'_i = (x'_i, y'_i, z'_i)$, determined from user-specified geometric targets. Thus, each landmark point had a known warping displacement defined as:

$$\mathbf{p}'_i = \mathbf{p}_i + d_{x,i} \cdot \mathbf{e}_1 + d_{y,i} \cdot \mathbf{e}_2 + d_{z,i} \cdot \mathbf{e}_3 \quad (1)$$

where $\mathbf{e}_1, \mathbf{e}_2, \mathbf{e}_3$ are standard Cartesian unit vectors, and $d_{x,i}, d_{y,i}, d_{z,i}$ are components of the warping displacement associated with surface landmark i . Equivalently, all other nodes in the model had an unknown warping displacement and final position, related by Eq. (2):

$$\mathbf{p}'_I = \mathbf{p}_I + d_x(x_I, y_I, z_I) \cdot \mathbf{e}_1 + d_y(x_I, y_I, z_I) \cdot \mathbf{e}_2 + d_z(x_I, y_I, z_I) \cdot \mathbf{e}_3 \quad (2)$$

where d_x, d_y, d_z are components of the warping displacement, which are a function of position within the model, and are determined by interpolating the known warping displacements at the surface landmarks. In this study, multiquadratic interpolation was used [51,52]. As an example, displacement in the x direction (d_x) of a node located at coordinates (x, y, z) was computed from Eqs. (3.a), (3.b), and Eq. (4):

$$d_x(x, y, z) = \sum_i a_i(x, y, z) \cdot w_i \quad (3.a)$$

$$a_i = \sqrt{(x-x_i)^2 + (y-y_i)^2 + (z-z_i)^2 + R^2} \quad (3.b)$$

where R is a scaling function set to the average distance between landmark nodes in the model, and w_i are a set of weights associated

with each landmark, calculated from linear interpolation constraints:

$$\begin{bmatrix} d_{x-1} \\ \vdots \\ d_{x-n} \end{bmatrix} = \begin{bmatrix} a_1(\mathbf{p}_1) & \cdots & a_1(\mathbf{p}_n) \\ \vdots & \ddots & \vdots \\ a_n(\mathbf{p}_1) & \cdots & a_n(\mathbf{p}_n) \end{bmatrix} \cdot \begin{bmatrix} w_1 \\ \vdots \\ w_n \end{bmatrix} \quad (4)$$

In this study, mesh morphing was performed based on physiologically realistic geometric extents. From previous literature, a realistic minimum and maximum value was selected for each geometric parameter (Table 1). When available, we considered the full range of values reported in the referenced studies. If only mean and standard deviation were reported, or if the number of specimens was relatively small (100), the realistic range was selected to be two standard deviations below and above the mean.


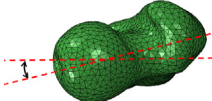
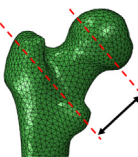



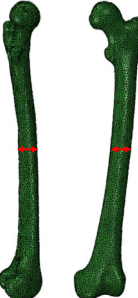
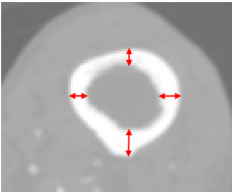
2.3. Preliminary sensitivity analysis

A preliminary sensitivity analysis was first conducted using one femur model. The goal was to assess whether any of the eight geometric parameters, discussed above, could be neglected in future analyses. The sensitivity analysis also revealed whether any of the geometric parameters had a strong nonlinear effect on strain, which might influence the choice of statistical model used in future sections.

Geometric parameters were varied across the full physiologically realistic range identified in Table 1. The mesh morphing algorithm was used to independently adjust each geometric parameter to five evenly spaced levels encompassing this range, while holding all other geometric parameters constant at the population mean.

This preliminary investigation revealed that NSA and FL had a relatively small influence on peak strains, with changes <2% different, relative to a model morphed to the population mean (Supplementary Fig. A.1). Thus, these parameters were neglected from future analyses. Moreover, all variables had a strong linear monotonic relationship to

Table 1
Visualization of the eight geometric parameters investigated in this study (MIDDLE) and summary of their physiologically realistic extents (RIGHT). For each geometric parameter, the range reported in this table encompasses the full range of values reported across all referenced studies.

Geometric measure	Visual example	Physiological extents
NSA		100°–146° Cadaveric measurements [42,45] 3D CT [46] 2D Radiographs [11]
NV		−2°–39° Cadaveric measurements [42] 3D CT [47,48]
NL		26–62 mm Cadaveric measurements [42]
FL		367–488 mm Cadaveric measurements [42]
L.Bow		−5°–16° 2D radiographs [14,16,49]
A.Bow		1°–23° 2D radiographs [16,50]
S.Dia		21–37 mm Cadaveric measurements [44]
C·Th	<p>Averaged from measurements in coronal and sagittal plane</p>  <p>Averaged over 4 locations</p>	3–6 mm Cadaveric measurements [44]

peak strain ($R^2 > 0.94$), suggesting that it was unnecessary to model a large array of intermediate values for each geometric parameter.

2.4. 2-Level full factorial analysis

Based on the preliminary findings from the sensitivity study, we designed a larger array of test cases in order to assess the influence of each geometric parameter across a wide range of realistic geometries. In this study, a 2-level full factorial design was implemented. Each geometric parameter was morphed to one of two levels, either the minimum or maximum physiologically realistic value (Table 1). Every possible permutation of high and low levels, across the six geometric parameters, was investigated. Thus, a total of 64 different geometries were simulated from each of the 10 femurs, for a total of 640 cases.

In each case, the peak von Mises strain in the proximal half of the shaft was recorded, and statistical analysis was performed using SPSS. Each case was associated with 21 independent variables, i.e., 6 geometric parameters plus all 15 first order interactions. These interactions were computed using Eq. (5.a) [53]:

$$(a \times b)_i = (a_i - \bar{a}) \cdot (b_i - \bar{b}) \quad (5.a)$$

where a and b are any two geometric parameters explored in this analysis, a_i and b_i are the values these parameters were assigned for the i th simulation case, and $(a \times b)_i$ is the interaction term between a and b for the i th simulation case. The average value of each interaction parameter across all 640 cases, \bar{a} and \bar{b} , were computed using Eq. (5.b):

$$\bar{a} = \frac{\sum_{i=1}^N a_i}{N}; \bar{b} = \frac{\sum_{i=1}^N b_i}{N} \quad (5.b)$$

where $N = 640$ is the total number of simulation cases in this study. A Generalized Estimating Equation (GEE, under GENLIN procedure in SPSS v.24) was used to assess the statistical significance of each independent variable in relation to peak von Mises equivalent strain and strained volume, while controlling for the correlated nature of our observations, i.e., 10 different native femora were morphed to the same 64 target geometries. Statistical significance of each parameter was evaluated at a criterion alpha-level of 0.05. Regression coefficients were also compared, in order to assess the relative impact of each parameter. To facilitate comparisons, coefficients were normalized by the range (max-min, Table 1) of their corresponding independent variable. This normalized coefficient represents the average change in strain or strained volume, measured from a wide range of varying geometries, expected when morphing from the minimum value of a parameter to the maximum.

3. Results

The pattern of deformation was similar among all models investigated, with elevated tensile strains along the lateral cortex (Fig. 3). However, geometry was found to have an impact on the vertical location of peak strain, with the largest effects from A.Bow (40%; $p < 0.001$), S.Dia (46%; $p < 0.001$), L.Bow (12%; $p < 0.001$), and A.Bow \times C.Th (9.2%; $p < 0.001$) (Fig. 4; Bottom).

Geometry also had important effects on peak strain and strained volume. As expected, all six geometric parameters had a statistically significant effect on peak femoral strains ($p \leq 0.05$; Fig. 4). The action of these variables was not wholly independent, with seven of fourteen interaction terms having statistically significant effects on peak von Mises strain ($p < 0.001$). Normalized regression coefficients from the 640 cases are illustrated in Fig. 4 (TOP). S.Dia had the largest effect on

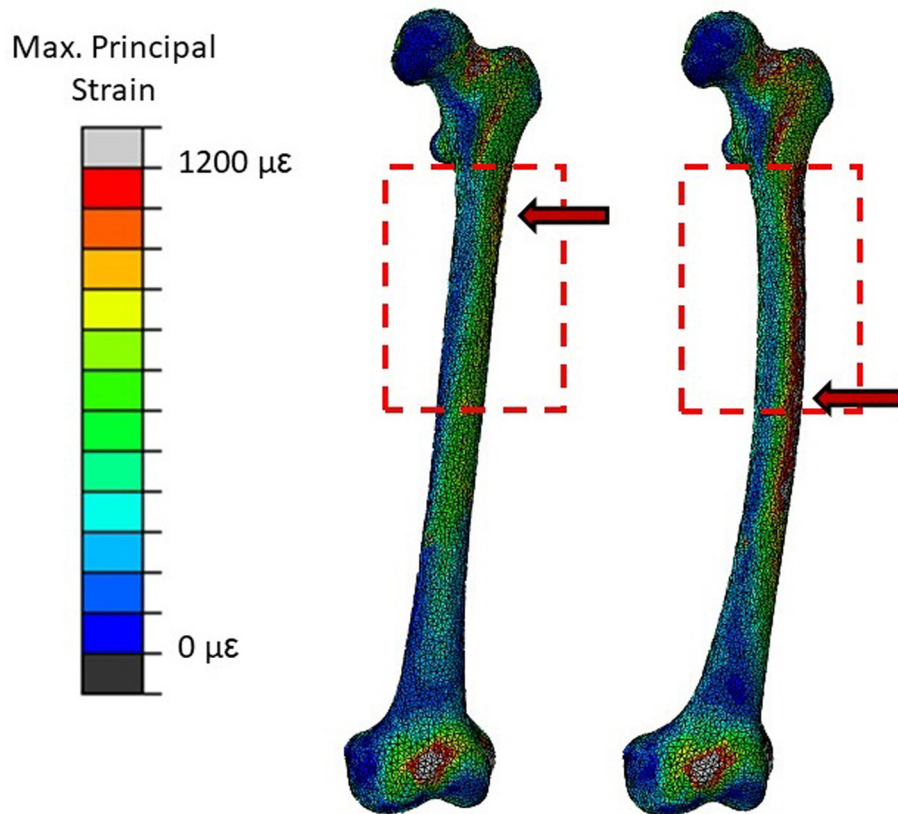


Fig. 3. Pattern of strain distribution from two representative models. As expected, models predicted elevated principal strains along the lateral aspect of the shaft. A dashed, red line shows the region of interest, and a red arrow notes the location of peak strain within this region. Peak strain typically occurred just below the lesser trochanter (LEFT) or near the midshaft (RIGHT).

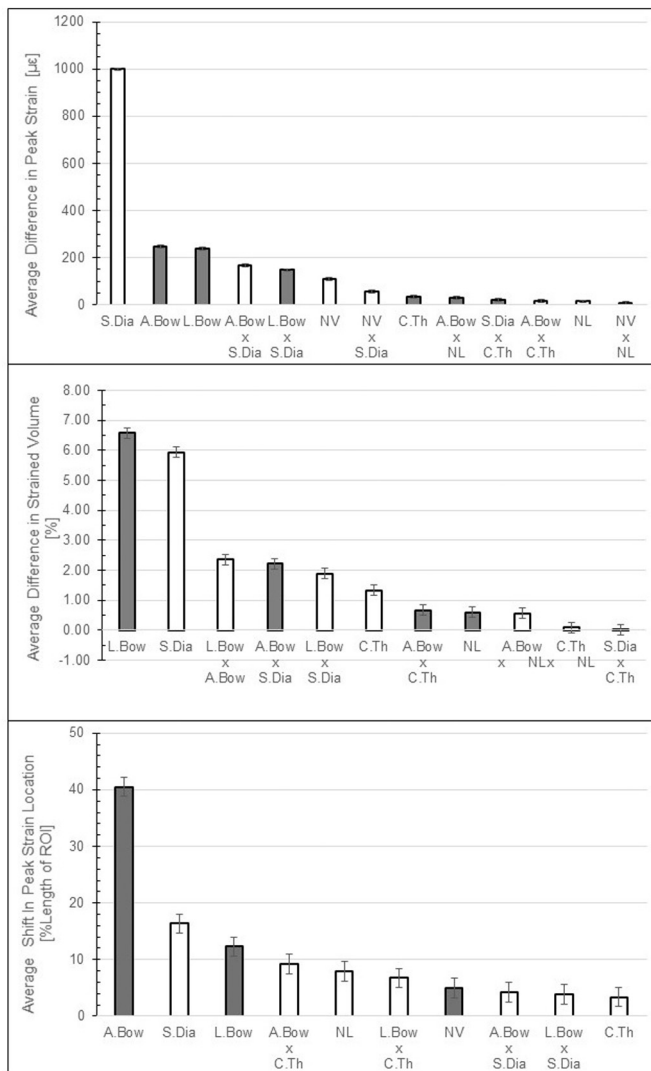


Fig. 4. Normalized regression coefficients from a 2-Level Full Factorial analysis. These coefficients represent the average change in peak strain (TOP), strained volume (MIDDLE) and vertical location of peak strain (BOTTOM) for any geometry morphed from the minimum to the maximum physiologically realistic value of the parameter. Only coefficients from statistically significant ($p < 0.05$) parameters are shown. Error bars show the standard error associated with each coefficient, which was very small for peak strain ($<1\%$ of the coefficient value). Positive relationships are shown in gray, with negative relationships in white.

peak strain ($998 \mu\epsilon$; $p < 0.001$) by a large margin, followed by A.Bow ($246 \mu\epsilon$; $p < 0.001$) and L.Bow ($236 \mu\epsilon$; $p < 0.001$). The two most impactful interactions were A.Bow \times S.Dia ($166 \mu\epsilon$; $p < 0.001$) and L.Bow \times S.Dia ($147 \mu\epsilon$; $p < 0.001$). Changing geometry also had a strong impact on strained volume. L.Bow had the largest impact on this parameter (6.7% ; $p < 0.001$) followed by S.Dia (5.9% ; $p < 0.001$). A.Bow, analyzed as an independent parameter, was not significant in this case; however, A.Bow was a component of the two most impactful interaction terms: A.Bow \times S.Dia (2.22% ; $p < 0.001$) and L.Bow \times A.Bow (2.36% ; $p < 0.001$) and (Fig. 4; MIDDLE).

4. Discussion

Femoral geometry is believed to play an important role in AFF. It is hypothesized that AFF is a mechanical fatigue phenomenon [5–7], and that certain geometries increase risk by elevating strains in the femoral shaft. Thus, the purpose of this study was to thoroughly quantify the relationship between femoral geometry and proximal femoral shaft strain. More specifically, we investigated the influence of eight

independent geometric parameters and their interactions on peak strain and strained volume at the proximal shaft. To do so, an algorithm was developed, which allowed for parametric morphing of specimen specific FE models. These models were simulated under physiologically relevant boundary conditions simulating the stance phase of gait. As expected, the study found that all six geometric parameters included in the 2-Level Full Factorial Analysis had a statistically significant ($p < 0.05$) effect on both peak strain and strained volume. Moreover, the action of these parameters were not wholly independent, with seven significant interaction terms being identified for peak strain, and a different seven interaction terms for strained volume.

All models experienced elevated principle strains along the lateral aspect of the femoral shaft (Fig. 3), and this strain distribution pattern is consistent with previously reported FE simulations [14,28,29,54,55]. In this study, however, we also found that morphing femoral geometry often shifted the location of peak von Mises equivalent strain, with A.Bow, S.Dia and L.Bow having the greatest effects. Recent investigations have explored the effect of bowing angle on AFF location, and concluded that patients with bowed femora were more likely to suffer a midshaft fracture, instead of a subtrochanteric fracture [14,16]. These findings are further supported by the results of our FE model predictions.

Femoral geometry also influenced the magnitude of peak von Mises strain, with S.Dia, L.Bow, and A.Bow and L.Bow \times S.Dia having the greatest effects. These results were extremely consistent across the individual specimens, and the standard error for all normalized regression coefficients was $<1\%$ (Fig. 4). The relative importance of the L.Bow parameter is consistent with previous literature, where an association between L.Bow and AFF is well established. Clinical investigations have suggested that this parameter can influence both AFF prevalence [11] and fracture location [49]. The remaining three parameters, however, have not been well studied in the clinical literature. In particular, A.Bow is likely neglected because it is not possible to measure using traditional coronal plane radiography. However, new imaging technologies like EOS make it feasible to explore all four of these most sensitive parameters in future clinical investigations.

With regard to the effect of femoral geometry on strained volume, this study found that L.Bow and S.Dia were the two most important parameters, respectively (Fig. 4). Surprisingly, A.Bow did not have a statistically significant impact on strained volume directly, but did appear as an interaction term in the third and fourth most important parameters, L.Bow \times A.Bow and A.Bow \times S.Dia. Considered alongside the findings in peak strain, these results suggest that a single geometric measurement, such as L.Bow, may be insufficient to detect variations in femoral diaphyseal strains. This conclusion is more readily apparent when quantitatively assessing the findings from Morin et al. [11], who previously reported statistically significant differences in L.Bow of AFF patients compared to unfractured controls. This study reported that an average L.Bow increase of only 2.4° discriminated fracture prevalence. Based on the model developed in this study, however, we found that such a small difference in L.Bow would only account for a difference in femoral shaft strain of approximately $23 \mu\epsilon$. This is only 1.1% of the median peak strain ($2092 \mu\epsilon$) predicted in the 640 test cases modeled in this study. It is difficult to conclude that such a small difference in strain alone could account for an increased risk of AFF.

It is important to note that our findings related to changes in L.Bow and femoral strain do not disprove the hypothesis that AFF risk is linked to elevated femoral diaphyseal strains. The observed differences in L.Bow may be correlated with a number of other, unmeasured, geometric changes which together cause nontrivial increase in femoral strains. For example, Kim et al. [56] found that L.Bow and A.Bow are highly correlated in AFF patients, and that AFF initiation site was dependent on femoral geometry. Similarly, a recent modelling study by Oh et al. [14] found that fracture sites in AFF corresponded to regions of high strain. Together, these previous studies suggest that the etiology of AFF is dependent, at least in part, on the mechanical environment of the femur and is not purely a rare biological response to BP medication. It remains

plausible, however, that the observed association between AFF risk and femoral geometry is due to factors other than strain. For example, it is not well understood whether subtle differences in femoral geometry have an appreciable effect on the joint contact and muscle forces associated with gait and other activities of daily living. It is also plausible that differences in patient femoral geometry are correlated in some way to differences in the underlying biological response to BP therapy, and that these differences play a role in AFF risk.

To the best of our knowledge, this is the first investigation to thoroughly quantify the relationship between femoral geometry and strain, and the use of parametric mesh morphing was an important strength of this work. The overall influence of each geometric parameter was explored through a robust 2-Level Full Factorial analysis; this analysis allowed us to quantify the relative importance of each geometric parameter across a wide array of physiologically realistic femoral shapes. It would be extremely challenging to achieve similar results by only imaging real patients, as it is unlikely that we could sample the full range of geometric variation possible across the entire population.

There are some noteworthy limitations that should be discussed when interpreting the results of this study. We investigated strains under only a single load case, i.e., walking. This case was selected because it is likely the most commonly repeated activity performed by individuals at risk of developing AFF. Moreover, a recent study [54] investigated strain patterns from a number of different loading activities and concluded that walking was likely the most relevant activity for the development of AFF. Next, although this work was able to identify the relative importance of different geometric parameters and their interactions on femoral strain, it was unable to quantitatively determine thresholds for AFF risk. The parametric examination was also unable to identify whether certain geometric parameters are correlated in the clinical population. Both of these questions can only be answered through clinical investigations, which are planned as future work. The statistical analysis performed in this work, while powerful, may be sensitive to errors in our chosen parameters space. It remains challenging to precisely identify the physiological extents of geometric parameters in the population as a whole. Demographics may influence femoral geometry, and the studies referred to in this work looked at very different populations. However, the strong linearity of the strain response with respect to all geometric parameters observed herein (Fig. A.1), suggests that errors in the minimum and maximum level used in the 2 Level Full Factorial analysis would not have a strong impact on the overall conclusions of this study.

Finally, in this work, we used results from a linear elastic model under monotonic loading to draw conclusions about risk of AFF. AFF is hypothesized to be a fatigue-driven failure event, i.e., a nonlinear process in which damage accumulates over repetitive loads until a critical threshold is exceeded, and the structure fails. However, we are not aware of any validated non-linear FE models which accurately simulate this process at the bone organ level. Instead, the models presented here provide information about the strain amplitude in different regions of the femur. It is well-established that fatigue life of bone is highly dependent on strain amplitude [38], and we expect that elevated FE strain predictions are associated with decreased fatigue life and increased AFF risk. This is analogous to the stress-life approach often used to study structures made from more traditional engineering materials [57]. As a result, this type of FE analysis has been used successfully in the past to draw meaningful conclusions about AFF [14,54].

5. Conclusions

As expected, changes to femoral geometry can have an impact on strains in the femoral diaphysis. Respectively, S.Dia and L.Bow had the largest impact on both femoral diaphyseal strain magnitude and strained volume. This study also found that considering geometric parameters independently may provide an incomplete assessment of AFF risk. Indeed, seven different interaction terms had significant effects

on both peak strain and strained volume. Clinical studies have demonstrated that relatively small changes to a single geometric parameter (L.Bow) can discriminate between AFF and unfractured controls [11]. However, if only this single parameter differs, the model developed herein predicts a small increase of only 23 $\mu\epsilon$, on average, between the two groups. This is only 1.1% of the median peak strain predicted in the 640 simulations used in this study. Future work is necessary to determine whether AFF patients have a number of correlated geometric differences which, together, cause a larger difference in femoral shaft strain. Work is also needed to better quantify the relationship between increased strain and AFF risk, and determine whether FE predicted shaft strains can be used to predict AFF prevalence.

Supplementary data to this article can be found online at <https://doi.org/10.1016/j.bone.2018.02.015>.

Acknowledgements

This work was funded in part by a Clinician-Scientist Collaboration Seed Grant from the McCaig Institute for Bone and Joint Health, Section of Orthopaedics and Division of Rheumatology, Cumming School of Medicine, University of Calgary. We would also like to thank Dr. Tak Fung, who provided advice on the statistical analysis methods used in this work.

References

- [1] A. Papaioannou, S. Morin, A.M. Cheung, S. Atkinson, J.P. Brown, S. Feldman, et al., 2010 clinical practice guidelines for the diagnosis and management of osteoporosis in Canada: summary, *CMAJ* 182 (2010) 1864–1873, <https://doi.org/10.1503/cmaj.100771>.
- [2] M.D.S.R. Cummings, M.D.J.S. Martin, M.D.M.R. McClung, M.D.E.S. Siris, M.D.R. Eastell, M.D.I.R. Reid, et al., Denosumab for prevention of fractures in postmenopausal women with osteoporosis, *N. Engl. J. Med.* 361 (2009) 756–765, <https://doi.org/10.1056/NEJMoa0809493>.
- [3] D.M. Black, P.D. Delmas, R. Eastell, I.R. Reid, S. Boonen, J.A. Cauley, et al., Once-yearly Zoledronic acid for treatment of postmenopausal osteoporosis, *N. Engl. J. Med.* 356 (2007) 1809–1822, <https://doi.org/10.1056/NEJMoa067312>.
- [4] E. Shane, D. Burr, B. Abrahamsen, R.A. Adler, T.D. Brown, A.M. Cheung, et al., Atypical subtrochanteric and diaphyseal femoral fractures: second report of a task force of the American society for bone and mineral research, *J. Bone Miner. Res.* 29 (2014) 1–23, <https://doi.org/10.1002/jbmr.1998>.
- [5] C.J. Hernandez, M.C.H. van der Meulen, Understanding bone strength is not enough, *J. Bone Miner. Res.* 32 (2017) 1157–1162, <https://doi.org/10.1002/jbmr.3078>.
- [6] E. Donnelly, A. Saleh, A. Unnanuntana, J.M. Lane, Atypical femoral fractures: epidemiology, etiology, and patient management, *Curr Opin Support Palliat Care* 6 (2012) 348–354, <https://doi.org/10.1097/SPC.0b013e3283552d7d>.
- [7] C. Kayali, T. Altay, F. Ozan, S. Sozkesen, K. Yamak, Atypical femoral shaft fractures secondary to long-term bisphosphonate therapy, *J. Orthop.* 14 (2017) 226–230, <https://doi.org/10.1016/j.jor.2017.01.002>.
- [8] B. Ettinger, D.B. Burr, R.O. Ritchie, Proposed pathogenesis for atypical femoral fractures: lessons from materials research, *Bone* 55 (2013) 495–500, <https://doi.org/10.1016/j.bone.2013.02.004>.
- [9] F. Chen, Z. Wang, T. Bhattacharyya, Absence of femoral cortical thickening in long-term bisphosphonate users: implications for atypical femur fractures, *Bone* 62 (2014) 64–66, <https://doi.org/10.1016/j.bone.2014.01.011>.
- [10] J.H. Koh, J.P. Myong, J. Yoo, Y.-W. Lim, J. Lee, S.-K. Kwok, et al., Predisposing factors associated with atypical femur fracture among postmenopausal Korean women receiving bisphosphonate therapy: 8 years' experience in a single center, *Osteoporos. Int.* (2017) <https://doi.org/10.1007/s00198-017-4169-y>.
- [11] S.N. Morin, M. Wall, E.L. Belzile, B. Godbout, T.P. Moser, L. Michou, et al., Assessment of femur geometrical parameters using EOS (TM) imaging technology in patients with atypical femur fractures: preliminary results, *Bone* 83 (2016) 184–189, <https://doi.org/10.1016/j.bone.2015.10.016>.
- [12] P. Franceschetti, M. Bondanelli, G. Caruso, M. Rosaria, V. Lorusso, M. Chiara, et al., Risk factors for development of atypical femoral fractures in patients on long-term oral bisphosphonate therapy, *Bone* 56 (2013) 426–431, <https://doi.org/10.1016/j.bone.2013.07.010>.
- [13] D.P. Taormina, A.I. Marcano, R. Karia, K.A. Egol, N.C. Tejwani, Symptomatic atypical femoral fractures are related to underlying hip geometry, *Bone* 63 (2014) 1–6, <https://doi.org/10.1016/j.bone.2014.02.006>.
- [14] Y. Oh, K. Fujita, Y. Wakabayashi, Y. Kurosa, A. Okawa, Location of atypical femoral fracture can be determined by tensile stress distribution influenced by femoral bowing and neck-shaft angle: a CT-based nonlinear finite element analysis model for the assessment of femoral shaft loading stress, *Injury* 48 (2017) 2736–2743, <https://doi.org/10.1016/j.injury.2017.09.023>.
- [15] Y. Oh, Y. Wakabayashi, Y. Kurosa, K. Fujita, A. Okawa, Potential pathogenic mechanism for stress fractures of the bowed femoral shaft in the elderly: mechanical

- analysis by the CT-based finite element method, *Injury* 45 (2014) 1764–1771, <https://doi.org/10.1016/j.injury.2014.08.037>.
- [16] J.W. Kim, J.J. Kim, Y.S. Byun, O.J. Shon, H.K. Oh, K.C. Park, et al., Factors affecting fracture location in atypical femoral fractures: a cross-sectional study with 147 patients, *Injury* 48 (2017) 1570–1574, <https://doi.org/10.1016/j.injury.2017.05.033>.
 - [17] I.T. Haider, A.D. Speirs, H. Frei, Effect of boundary conditions, impact loading and hydraulic stiffening on femoral fracture strength, *J. Biomech.* 46 (2013) 2115–2121, <https://doi.org/10.1016/j.jbiomech.2013.07.004>.
 - [18] W.B. Edwards, T.J. Schnitzer, K.L. Troy, Torsional stiffness and strength of the proximal tibia are better predicted by finite element models than DXA or QCT, *J. Biomech.* 46 (2013) 1655–1662, <https://doi.org/10.1016/j.jbiomech.2013.04.016>.
 - [19] L. Grassi, E. Schileo, F. Taddei, L. Zani, M. Jusczyk, L. Cristofolini, et al., Accuracy of finite element predictions in sideways load configurations for the proximal human femur, *J. Biomech.* 45 (2012) 394–399, <https://doi.org/10.1016/j.jbiomech.2011.10.019>.
 - [20] C. Xu, A. Silder, J. Zhang, J. Hughes, G. Unnikrishnan, J. Reifman, et al., An integrated musculoskeletal-finite-element model to evaluate effects of load carriage on the tibia during walking, *J. Biomech. Eng.* 138 (2016), 101001, <https://doi.org/10.1115/1.4034216>.
 - [21] I.A. Sigal, H. Yang, M.D. Roberts, J.C. Downs, Morphing methods to parameterize specimen-specific finite element model geometries, *J. Biomech.* 43 (2010) 254–262, <https://doi.org/10.1016/j.jbiomech.2009.08.036>.
 - [22] R. Hambli, S. Allaoui, A robust 3D finite element simulation of human proximal femur progressive fracture under stance load with experimental validation, *Ann. Biomed. Eng.* (2013) <https://doi.org/10.1007/s10439-013-0864-9>.
 - [23] E. Schileo, L. Balistreri, L. Grassi, L. Cristofolini, F. Taddei, To what extent can linear finite element models of human femora predict failure under stance and fall loading configurations? *J. Biomech.* 47 (2014) 3531–3538, <https://doi.org/10.1016/j.jbiomech.2014.08.024>.
 - [24] J.H. Keyak, Improved prediction of proximal femoral fracture load using nonlinear finite element models, *Med. Eng. Phys.* 23 (2001) 165–173.
 - [25] E. Schileo, F. Taddei, A. Malandrino, L. Cristofolini, M. Viceconti, Subject-specific finite element models can accurately predict strain levels in long bones, *J. Biomech.* 40 (2007) 2982–2989, <https://doi.org/10.1016/j.jbiomech.2007.02.010>.
 - [26] J.H. Keyak, I.Y. Lee, H.B. Skinner, Correlations between orthogonal mechanical properties and density of trabecular bone: use of different densitometric measures, *J. Biomed. Mater. Res.* 28 (1994) 1329–1336.
 - [27] W.B. Edwards, R.H. Miller, T.R. Derrick, Femoral strain during walking predicted with muscle forces from static and dynamic optimization, *J. Biomech.* 49 (2016) 1206–1213, <https://doi.org/10.1016/j.jbiomech.2016.03.007>.
 - [28] A.D. Speirs, M.O. Heller, G.N. Duda, W.R. Taylor, Physiologically based boundary conditions in finite element modelling, *J. Biomech.* 40 (2007) 2318–2323, <https://doi.org/10.1016/j.jbiomech.2006.10.038>.
 - [29] G.N. Duda, M. Heller, J. Albinger, O. Schulz, E. Schneider, L. Claes, Influence of muscle forces on femoral strain distribution, *J. Biomech.* 31 (1998) 841–846.
 - [30] A. Aamodt, J. Lund-Larsen, J. Eine, E. Andersen, P. Benum, O.S. Husby, In vivo measurements show tensile axial strain in the proximal lateral aspect of the human femur, *J. Orthop. Res.* 15 (1997) 927–931, <https://doi.org/10.1002/jor.1100150620>.
 - [31] J.J. Kruzic, R.O. Ritchie, Fatigue of mineralized tissues: cortical bone and dentin, *J. Mech. Behav. Biomed. Mater.* 1 (2008) 3–17, <https://doi.org/10.1016/j.jmbbm.2007.04.002>.
 - [32] L. Rapillard, M. Charlebois, P.K. Zysset, Compressive fatigue behavior of human vertebral trabecular bone, *J. Biomech.* 39 (2006) 2133–2139, <https://doi.org/10.1016/j.jbiomech.2005.04.033>.
 - [33] F.M. Lambers, A.R. Bouman, C.M. Rimnac, C.J. Hernandez, Microdamage caused by fatigue loading in human cancellous bone: relationship to reductions in bone biomechanical performance, *PLoS One* 8 (2013), e83662, <https://doi.org/10.1371/journal.pone.0083662>.
 - [34] T.L. Moore, L.J. Gibson, Fatigue of bovine trabecular bone, *J. Biomech. Eng.* 125 (2003) 761, <https://doi.org/10.1115/1.1631583>.
 - [35] G.R. Brock, J.T. Chen, A.R. Ingrassia, J. MacLeay, G.E. Pluhar, A.L. Boskey, et al., The effect of osteoporosis treatments on fatigue properties of cortical bone tissue, *Bone Reports* 2 (2015) 8–13, <https://doi.org/10.1016/j.bonr.2014.10.004>.
 - [36] D.G. Kim, M.A. Miller, K.A. Mann, A fatigue damage model for the cement-bone interface, *J. Biomech.* 37 (2004) 1505–1512, <https://doi.org/10.1016/j.jbiomech.2004.01.011>.
 - [37] J.H. Kim, M. Niinomi, T. Akahori, H. Toda, Fatigue properties of bovine compact bones that have different microstructures, *Int. J. Fatigue* 29 (2007) 1039–1050, <https://doi.org/10.1016/j.ijfatigue.2006.09.018>.
 - [38] D.R. Carter, W.E. Caler, D.M. Spengler, V.H. Frankel, Fatigue behavior of adult cortical bone: the influence of mean strain and strain range, *Acta Orthop.* 52 (1981) 481–490, <https://doi.org/10.3109/17453678108992136>.
 - [39] R.H.J. Peerlings, R. De Borst, W.A.M. Brekelmans, J.H.P. De Vree, Gradient enhanced damage for quasi-brittle materials, *Int. J. Numer. Methods Eng.* 39 (1996) 3391–3403.
 - [40] D. Taylor, F. O'Brien, A. Prina-Mello, C. Ryan, P. O'Reilly, T.C. Lee, Compression data on bovine bone confirms that a “stressed volume” principle explains the variability of fatigue strength results, *J. Biomech.* 32 (1999) 1199–1203, [https://doi.org/10.1016/S0021-9290\(99\)00112-8](https://doi.org/10.1016/S0021-9290(99)00112-8).
 - [41] J. Schilcher, Howe T. Sen, M.A. Png, P. Aspenberg, J.S.B. Koh, Atypical fractures are mainly subtrochanteric in Singapore and Diaphyseal in Sweden: a cross-sectional study, *J. Bone Miner. Res.* 30 (2015) 2127–2132, <https://doi.org/10.1002/jbmr.2547>.
 - [42] M. Verma, S. Joshi, A. Tuli, S. Raheja, P. Jain, P. Srivastava, Morphometry of proximal femur in Indian population, *J. Clin. Diagn. Res.* 11 (2017) AC01–AC04, <https://doi.org/10.7860/JCDR/2017/23955.9210>.
 - [43] M.D. Hellman, B.D. Haugom, N.M. Brown, Y.A. Fillingham, M.J. Philippon, S.J. Nho, Femoroacetabular impingement and pelvic incidence: radiographic comparison to an asymptomatic control, *Arthrosc. J. Arthrosc. Relat. Surg.* 33 (2017) 545–550, <https://doi.org/10.1016/j.arthro.2016.08.033>.
 - [44] R.B. Martin, P.J. Atkinson, Age and sex-related changes in the structure and strength of the human femoral shaft, *J. Biomech.* 10 (1977) 223–231, [https://doi.org/10.1016/0021-9290\(77\)90045-8](https://doi.org/10.1016/0021-9290(77)90045-8).
 - [45] I. Gilligan, S. Chandraphak, P. Mahakkanukrauh, Femoral neck-shaft angle in humans: variation relating to climate, clothing, lifestyle, sex, age and side, *J. Anat.* 223 (2013) 133–151, <https://doi.org/10.1111/joa.12073>.
 - [46] M.J. Hartel, A. Petersik, A. Schmidt, D. Kendoff, J. Nüchtern, J.M. Rueger, et al., Determination of femoral neck angle and torsion angle utilizing a novel three-dimensional modeling and analytical technology based on CT datasets, *PLoS One* 11 (2016) 1–10, <https://doi.org/10.1371/journal.pone.0149480>.
 - [47] N. Jiang, L. Peng, M. Al-Qwbani, G.-P. Xie, Q.-M. Yang, Y. Chai, et al., Femoral version, neck-shaft angle, and acetabular Anteversion in Chinese Han population, *Medicine (Baltimore)* 94 (2015), e891, <https://doi.org/10.1097/MD.0000000000000891>.
 - [48] M. Worlicek, M. Weber, B. Craiovan, M. Wörner, F. Völlner, H.R. Springorum, et al., Native femoral anteversion should not be used as reference in cementless total hip arthroplasty with a straight, tapered stem: a retrospective clinical study, *BMC Musculoskelet. Disord.* 17 (2016), 399, <https://doi.org/10.1186/s12891-016-1255-9>.
 - [49] H. Yoo, Y. Cho, Y. Park, S. Ha, Lateral femoral bowing and the location of atypical femoral fractures, *Hip Pelvis* 29 (2017) 127, <https://doi.org/10.5371/hp.2017.29.2.127>.
 - [50] S. Sasaki, N. Miyakoshi, M. Hongo, Y. Kasukawa, Y. Shimada, Low-energy diaphyseal femoral fractures associated with bisphosphonate use and severe curved femur: a case series, *J. Bone Miner. Metab.* 30 (2012) 561–567, <https://doi.org/10.1007/s00774-012-0358-0>.
 - [51] R.E. Carlson, T.A. Foley, The parameter R2 in multiquadric interpolation, *Comput Math with Appl* 21 (1991) 29–42, [https://doi.org/10.1016/0898-1221\(91\)90123-L](https://doi.org/10.1016/0898-1221(91)90123-L).
 - [52] G.B. Wright, Radial Basis Function Interpolation: Numerical and Analytical Developments, Ph.D Dissertation, Department of Applied Mathematics, University of Colorado, 2003.
 - [53] L. Aiken, S. West, R. Reno, *Multiple Regression: Testing and Interpreting Interactions*, Sage, Thousand Oaks, California, USA, 1991.
 - [54] S. Martelli, P. Pivonka, P.R. Ebeling, Femoral shaft strains during daily activities: implications for atypical femoral fractures, *Clin. Biomech.* 29 (2014) 869–876, <https://doi.org/10.1016/j.clinbiomech.2014.08.001>.
 - [55] A. Gustafsson, J. Schilcher, L. Grassi, P. Aspenberg, H. Isaksson, Strains caused by daily loading might be responsible for delayed healing of an incomplete atypical femoral fracture, *Bone* 88 (2016) 125–130, <https://doi.org/10.1016/j.bone.2016.04.020>.
 - [56] J.W. Kim, J.J. Kim, Y.S. Byun, O.J. Shon, H.K. Oh, K.C. Park, et al., Factors affecting fracture location in atypical femoral fractures: a cross-sectional study with 147 patients, *Injury* 48 (2017) 1570–1574, <https://doi.org/10.1016/j.injury.2017.05.033>.
 - [57] O. Kayabaşı, E. Yüzbaşıoğlu, F. Erzinanlı, Static, dynamic and fatigue behaviors of dental implant using finite element method, *Adv. Eng. Softw.* 37 (2006) 649–658, <https://doi.org/10.1016/j.advengsoft.2006.02.004>.